2013

# Reducing uncertainty in fatigue life limits of turbine engine alloys

J M. Larson
*Wright-Patterson Air Force Base*, james.larsen@wpafb.af.mil

S K. Jha
*Universal Technology Corporation*

C J. Szczepanski
*Wright-Patterson Air Force Base*

M J. Caton
*Wright-Patterson Air Force Base*

R John
*Wright-Patterson Air Force Base*

***See next page for additional authors***

International Journal of Fatigue 57 (2013) 103–112

Contents lists available at SciVerse ScienceDirect

International Journal of Fatigue

journal homepage: www.elsevier.com/locate/ijfatigue

# Reducing uncertainty in fatigue life limits of turbine engine alloys

J.M. Larsen [a,*], S.K. Jha [b], C.J. Szczepanski [a], M.J. Caton [a], R. John [a], A.H. Rosenberger [a], D.J. Buchanan [c], P.J. Golden [a], J.R. Jira [a]

[a] U.S. Air Force Research Laboratory, Wright-Patterson Air Force Base, OH 45433, USA
[b] Universal Technology Corporation, 1270 North Fairfield Rd., Dayton, OH 45432, USA
[c] University of Dayton Research Institute (UDRI), Dayton, OH 45469, USA

ARTICLE INFO

*Article history:*
Received 15 June 2012
Received in revised form 21 January 2013
Accepted 23 January 2013
Available online 5 February 2013

*Keywords:*
Damage tolerance
Fatigue design
Gas turbines
Microstructures
Probabilistic analysis

ABSTRACT

In probabilistic design of materials for fracture-critical components in modern military turbine engines, a typical maximum design target risk (DTR) is $5 \times 10^{-8}$ component failures/engine flight hour. This metric underscores the essential role of *safety* in a design process that simultaneously strives to achieve performance, efficiency, reliability, and affordability throughout the life cycle of the engine. Traditionally, the design and life management approaches for engine materials have typically relied on extensive testing programs to produce large databases of fatigue data, from which statistically based life limits are derived by extrapolation from the mean fatigue behavior. However, we have found that the statistical behavior of fatigue lifetimes under a given test condition often exhibits a bimodal form, and that the trends in mean vs. minimum fatigue lifetime typically respond differently to loading or to microstructural variables. Under such circumstances, the underlying life-limiting mechanisms appear to exhibit a probabilistic microstructural hierarchy in fatigue resistance that is controlled by susceptibility of local microstructural neighborhoods to early damage and the growth of small cracks. These findings suggest that significant opportunities may exist for reductions in *uncertainty* in materials life-cycle prediction and management, if such hierarchies can be understood and controlled. This paper explores the potential implications of these findings, and a number of possible approaches are suggested for incorporating the insights of life-limiting fatigue into methods of integrated computational materials engineering (ICME) to support optimized life-cycle design of materials and components in turbine engines. Benefits of this approach appear to include substantial improvements in model accuracy, coupled with reduced requirements for materials testing, potentially leading to a significant reduction in the time and cost to develop, validate, transition, and implement new, more fatigue resistant alloys.

Published by Elsevier Ltd.

## 1. Introduction

### 1.1. A bright future for materials design

Looking to the future of turbine engine materials, it appears that there are many potential breakthroughs in the underlying science and technology of materials design that could offer important opportunities for improvement beyond today's engineering state-of-the-art. For example, future designs are likely to benefit from a wave of anticipated advancements in probabilistic modeling and simulation, micro-experimentation, high fidelity materials characterization, mechanism-based modeling, and information science and technology, all of which are areas of enhanced investment under a number of major new initiatives in science and technology [1–4]. Through unprecedented levels of model integration among a range of science and engineering disciplines, it should be possible to design future propulsion systems to be more adaptable to new usage requirements, to have higher fuel efficiency, to be inherently more reliable and verifiable, to be manufactured and certified more quickly, and to require far less logistics support over the system's full life cycle.

In the relatively near term, continuous recording of engine flight and performance data streams is expected to give operators and logisticians unsurpassed knowledge of the usage of individual engines. Using comprehensive engine performance and stress analysis models of the engine, one can then calculate location-specific stresses and temperatures in individual engine components for use in life analysis. In the longer term, it should be possible to use diagnostics of structural and materials health as part of a comprehensive philosophy of condition based management + prognosis (CBM+) [5–9]. In the longer term, a key goal is to pursue the concept of aircraft digital twin to represent the evolving health state of each individual asset [10].

* Corresponding author. Tel.: +1 9372551357.
*E-mail address:* james.larsen@wpafb.af.mil (J.M. Larsen).

0142-1123/$ - see front matter Published by Elsevier Ltd.
http://dx.doi.org/10.1016/j.ijfatigue.2013.01.012

Undergirding these forecasted advancements, the burgeoning field of integrated computational materials engineering (ICME) [11,12] is expected to enable game-changing materials-design concepts, including the ability to tailor location-specific material properties that are optimized to meet component-specific life-cycle design requirements. Perhaps the greatest underlying challenge for the science and engineering community, however, will be to exploit the full potential of a material's capabilities, while simultaneously assuring safety, reliability, *and affordability* over the entire system life cycle. In this regard, the growing importance of affordability was recently underscored in the US Air Force forecast report: *Technology Horizons, Essential Focus Areas for Air Force S and T Investment*, which noted that "...Air Force science and technology over the next decade will need to focus as much on advancing technologies that enable reduced Air Force operating costs as on technologies that support more traditional development of new systems or capabilities." [13].

To help meet such challenges, the engine structural design community is immersed in building, improving, and exploiting comprehensive probabilistic design tools for engine components (e.g., [14]). Underpinning such computer codes are the variabilities and uncertainties in the input parameters and data, including probabilistic descriptions of engine missions/loads, aerodynamic flow, thermal and stress analysis, combustion effects, and materials performance in harsh environments. At the structures and system level, new concepts for robust design [15] and prognosis [5] are emerging. In addition, recent advancements in Bayesian updating offers a rigorous approach to refine model accuracy based on continuous feedback from diagnostic, maintenance, and operational data [16]. While it may take decades to fully develop and implement the science and technology needed to achieve the vision outlined above, there are many incremental steps that can facilitate transition and which offer significant nearer-term benefits. Perhaps the key initial step is the adoption of a modular, risk-based modeling framework in which input data and assumptions are represented probabilistically. Under this scenario, each input to the system-level model would be represented by one or more submodels, which could be individually developed and validated. Thus, the set of models of the usage, structural response, and materials performance could be continually improved, as the underlying science advances from its current empirical representation to a more fundamental physics base. The intent of the current paper is to highlight an area of progress in understanding uncertainty in the fatigue lifetime of a selected titanium alloy and to outline related opportunities in the area of integrated computational materials engineering.

### *1.2. Case study: turbine engine materials – building on a history of design and operation*

Life-cycle management procedures used for today's advanced turbine engines have achieved a superb record of safety, and the underlying models and methods have evolved over decades of design and operation. This process has culminated in validated engineering standards of practice, supported by large databases of material properties. Consequently, these engineering practices are highly tolerant to variations and uncertainties in materials and structures, and catastrophic fatigue failures of components have been virtually eliminated. At the same time, owing largely to the mature age of some of the fleets, engine life-cycle costs are growing at an annual rate that is well above inflation, and this cost burden threatens to stifle efforts to recapitalize and modernize future engine fleets [17]. Given such affordability challenges, there is a growing need to reduce life-cycle costs for both legacy and future engines. However, history indicates that as much as 80% of an engine's life cycle cost is established during the design and early development of the engine, and the cost to correct design defects afterward becomes exponentially greater as development and deployment proceed [17].

Within the US Department of Defense, the decades of engine design and engineering experience have molded the specifications known as the Propulsion System Integrity Program (PSIP) [18] and its associated document [19], which guide the life-cycle design and management of turbine engines. The process of PSIP design, depicted schematically in Fig. 1, is the beginning of a comprehensive life-cycle design and logistics management process that includes: (i) design information and development planning; (ii) design characterization and analysis; (iii) components and subsystems testing; (iv) propulsion system ground and flight testing, and (v) the engine life management plan. Engine-material development, selection, characterization, modeling, and validation are concentrated in tasks (i) and (ii), and first-tier material properties,

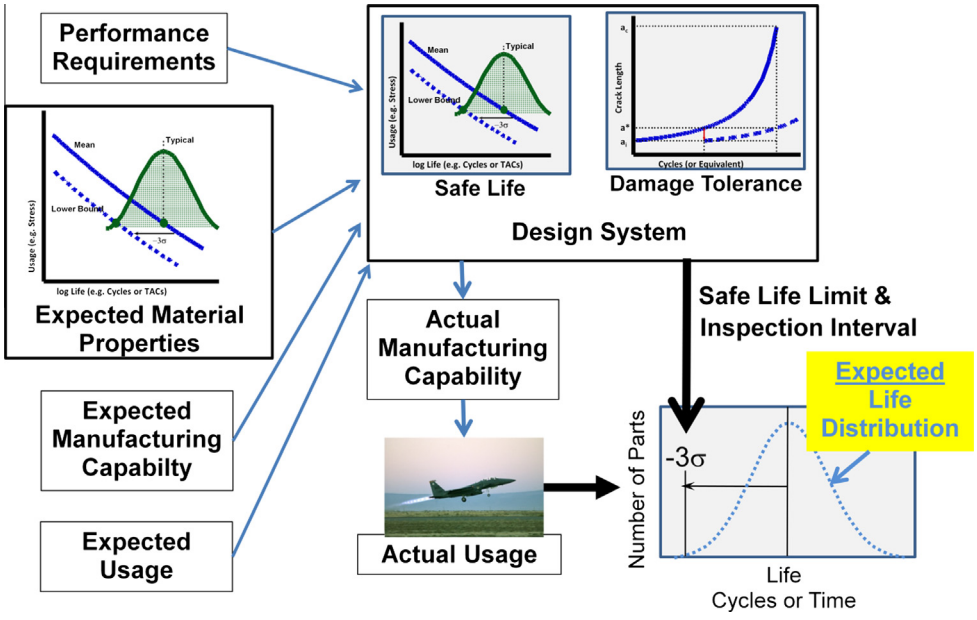


**Fig. 1.** Schematic of design requirements and expected material/component response specified by the Department of Defense Propulsion System Integrity Program (PSIP).

such as strength, stiffness, and density, tend to drive initial design. Second-tier material properties, such as cycle-, time-, temperature-, and environmental-dependence, are prominent factors throughout the design and life cycle, and these properties typically define engine overhaul intervals, control the average time on wing, and dictate the ultimate lifetimes of components.

For safety- or mission-critical components, such as rotors and rotor spacers, the PSIP design life is driven primarily by major load cycles produced by variations in engine rotational speed, wherein a ground-air-ground flight is counted as one cycle, and minor throttle excursions during flight count as partial cycles. Such cycles may be summarized as total accumulated cycles (TACs), and a typical flight produces approximately 2–3 TACs/h. To satisfy performance and safety requirements, a design life for major rotating components in high performance engines is nominally 8000 TACs, with a complete overhaul of the engine prescribed at 4000 TACs. Given these target lifetimes, the associated maximum stresses in rotor components tend to approach the material yield strength at key locations, such as boltholes and other stress concentrators, and relatively high maximum stresses occur throughout the components.

With regard to the materials life cycle, it is well known that advanced Ti and Ni alloys in turbine engine rotors exhibit a substantial variation in their long-term cyclic- and time-dependent properties, such as resistance to fatigue damage and, to a lesser extent, resistance to creep deformation. The PSIP specifications deal with such variation by managing to a criterion based on statistical lower-bound behavior. For example, for design of safety- or mission-critical components, these specifications impose simultaneous requirements for (i) a statistical minimum safe-life fatigue and (ii) damage tolerance to small surface or corner cracks. Under the safe-life criterion, the minimum LCF life is defined as −3 standard deviations from the mean value of the material's low cycle fatigue lifetime, or alternatively, the 1/1000 (B0.1) lower-bound capability, based on a database of tests over the range of engine design conditions. Thus, the PSIP specification virtually guarantees material safety under low cycle fatigue, although the reliance on large statistical databases can be costly and time consuming.

Engines are designed to meet targeted mission profiles of loads, but actual mission usage invariably changes as the operational needs change, making tracking of actual mission usage a key input to improved life analysis. Future engines are to be designed with sophisticated usage-tracking capabilities, and the stresses and temperatures of engine components are, therefore, expected to be much more well defined than is possible today. However, the understanding and control of variability in the material's response to such loading is much less mature, and represents a significant, although challenging, opportunity for improvement.

In the quest for improved models to address the goals of safety, reliability, and affordability, *safety* will certainly remain as the first requirement for manned aircraft. For example, as noted in the PSIP specification, the limit for the design target risk (DTR) for probabilistic design of a component "was set at a value of $5 \times 10^{-8}$ predicted occurrences per EFH [Engine Flight Hour] for a recent, advanced single-engine fighter." Similarly, specifications for commercial engine components set the maximum DTR at $1 \times 10^{-9}$/flight [20]. Such rigorous safety requirements underscore the importance of fatigue life limits in design and operation of turbine engines, and highlight the challenges facing integrated computational materials engineering for engine alloys.

### 1.3. Life limits and competing-mode of fatigue

Under previous efforts on life-limiting material behavior, we have found that the variability in fatigue response of engine alloys at a given stress level often tends to separate into bimodal distributions representing minimum behavior and a mean-life dominated behavior, termed Type I and Type II behavior, respectively. Thus, the probability density representing a material's safe-life fatigue capability, depicted in Fig. 1, was often composed of two underlying probability densities, as shown schematically in Fig. 2. This separation in fatigue lifetimes, known as bimodal or competing-modes fatigue, has been observed in a wide range of alloys, including the superalloys: Rene'95 [21,22], Rene'88DT [23], IN100 [8,24–29], Waspaloy [30], the single crystal alloy PWA 1484 [31], the titanium alloys Ti-10-2-3 [23,32–34], Ti–6Al–2Sn–4Zr–6Mo [35–42], Ti–6Al–4V [43–47], gamma titanium aluminides [48,49], the aluminum alloy 7075-T651 [50], and others. Although such a separation of fatigue response has been known for some time [51], the significance of this behavior has not yet been generally captured in the strategies for fatigue design of turbine engine materials.

In exploring this behavior in turbine engine alloys, we have developed a physically-based approach for describing fatigue variability, and this approach has been integrated into a Monte Carlo probabilistic life prediction model for materials [35,40,52]. The primary tenets of our fatigue variability description are summarized by [40]: (i) under nominal microstructural and loading conditions, a hierarchy of local deformation heterogeneities develop in a fatigue sample, corresponding to grain-scale cyclic micro-plasticity in certain microstructural arrangements or features; (ii) as a result of this hierarchy, a probability exists of an extreme microstructural arrangement that may initiate a crack-growth dominated failure, producing a life-limiting failure distribution for the material; and (iii) there are often different degrees of influence of a given variable on minimum vs. the mean lifetimes. For example, the effect of stress level on mean vs. life-limiting fatigue typically produces quite different responses, and such differing response of minimum and mean fatigue behavior has been observed for other important variables, including microstructure, surface treatment, temperature, and dwell time. Furthermore, this behavior appears to manifest itself in the presence of notches [53]. This understanding, when applied to fatigue design of materials, suggests that compositional, processing, surface treatment, and microstructural modifications should consider the lower-lifetime limit, and that the life-limiting behavior may not be accurately represented by purely statistical, mean-fatigue-based, approaches.

The goal of the current paper is to (i) overview general findings on fatigue life limits of alloys used in turbine-engine rotor

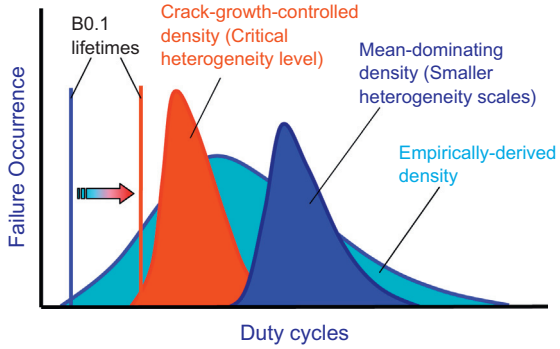


**Fig. 2.** Expanding on the concept of "Expected Material Properties" highlighted at the upper left of Fig. 1, it is commonly assumed that fatigue variability is well described by a single probability distribution (light blue), as show above. Traditional methods of design and life management derive material life limits by extrapolation to the lower tail of the single distribution. However, it now appears that such fatigue lifetime behavior may actually arise from at least two separate underlying probability distributions. In this sense, the identification of two distributions appears to offer substantial opportunity for improved understanding of the fundamental material behavior and a reduction in predictive uncertainty. (For interpretation of the references to colour in this figure legend, the reader is referred to the web version of this article.)

components, (ii) to highlight the effects and implications of such fatigue life limits for a specific high strength titanium alloy, and (iii) to identify possible avenues for improvement in materials-model accuracy. Thus, the focus will be on challenges and opportunities to reduce variability in performance, and uncertainty of predictions, of fatigue life-cycle capability of turbine-engine rotor materials, consistent with the demands of a high-performance single-engine aircraft.

## 2. Materials and experimental methods

The focus of this investigation was a pancake forging of alloy Ti–6Al–2Sn–4Zr–6Mo(Ti–6246) processed and heat-treated to a duplex $\alpha + \beta$ phase microstructural condition, as shown in Fig. 3. The microstructure consisted of primary, equiaxed $\alpha$ particles ($\alpha_p$), and lamellar colonies of fine $\alpha/\beta$ laths, which transformed from prior-β grains during heat treatment. The average size of the $\alpha_p$ was about 4 μm and that of the colonies was about 15 μm. The volume fractions of $\alpha_p$ and the colony phases were approximately 0.3 and 0.7, respectively. This produced a bulk yield strength of 1140 MPa and an ultimate strength of 1250 MPa.

Closely spaced, cylindrical specimen blanks of this material were machined from the forging, and sections of Ti–6Al–4V rod were inertia welded to the ends as extensions for gripping. Subsequently, the inertia-welded blanks were machined and finished by low-stress grinding into either cylindrical dog-bone specimens for fatigue testing, or similar small-crack specimens, which were fabricated with surface flats to accommodate crack growth measurements using standard acetate replication procedures. Surface residual stresses from machining were removed by electropolishing the machined specimens to remove a 50 μm thick surface layer on the specimen gage sections. The small-crack tests were performed using either natural initiation or by initiation from multiple small surface notches, which had been machined into the surface using a focused ion beam (FIB) to create residual-stress-free crack starters.

To assess the inherent effect of the Ti-6246 alloy microstructure on the variability in fatigue response, a series of tension–tension fatigue tests was performed at each of nine stress levels under a stress ratio of minimum/maximum stress of 0.05. The specific maximum stresses for these tests were 1040, 925, 900, 860, 820, 700, 650, 600, and 550 MPa. The test frequency was 20 Hz for maximum stresses above 750 MPa, while tests below this stress were performed in ultrasonic resonance at 20 kHz. At the highest stresses, surface-connected $\alpha$ particles typically served as the primary sites for crack initiation (e.g., Fig. 4), while some of the specimens failed from internal initiation sites under maximum stresses of 860 MPa or lower. Further details on the microstructure, experimental methods, results, and analysis are provided in [37,39–41,54], which served as the backbone of the results to be presented below.

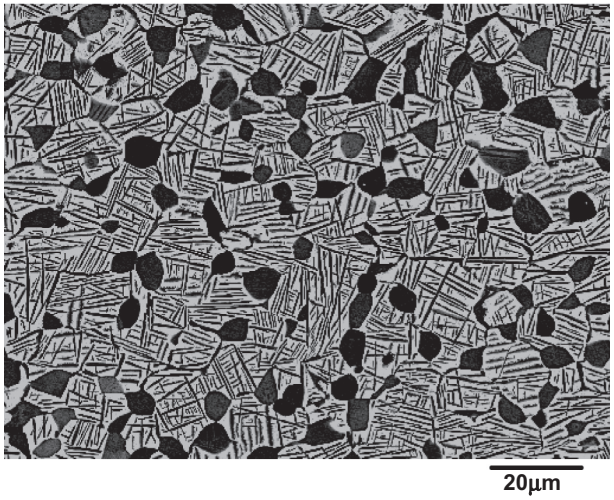


**Fig. 3.** Nominal duplex microstructure of Ti–6Al–2Sn–4Zr–6Mo alloy processed to in the $\alpha + \beta$ phase field, containing approximately 30% primary $\alpha$ grains and fine α-phase platelets in a matrix of transformed $\beta$ phase.

## 3. Results

Fig. 5 presents an *S–N* plot of the resulting fatigue lifetimes for all stress levels ($\sigma_{max}$ of 550–1040 MPa) and both frequencies. As shown, the variability in fatigue lifetime exceeded three orders of magnitude at the intermediate stress levels, while the variability in lifetime at the highest stress level (1040 MPa) was extremely limited. The increase in variability with reducing stress has been observed widely in the literature, although the extent of the increase is likely maximized for the current tests, due to the use of

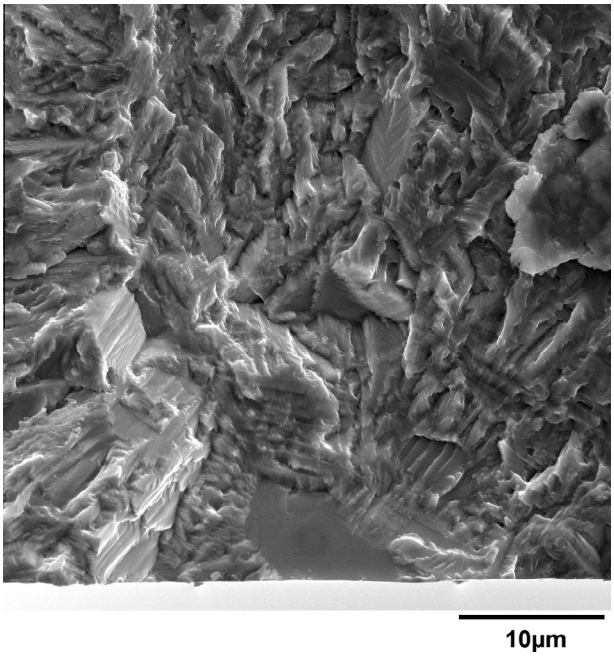


**Fig. 4.** Typical fatigue crack origin (lower edge) showing a single, surface-connected, alpha grain facet where crack nucleation occurred.

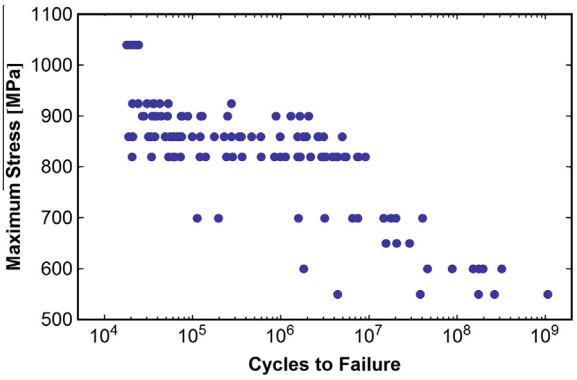


**Fig. 5.** Ti-6246 stress vs. life (*S–N*) with plot showing individual specimen lifetimes. Tests above 750 MPa performed at 20 Hz, and tests below 750 MPa performed at 20 kHz.

residual-stress-free electropolished surfaces. This surface condition was chosen, however, precisely because it eliminated effects of surface irregularities and residual stresses and helped to reveal the inherent effects of alloy microstructure. The nature of the statistical variations in the fatigue lifetimes at each stress level is elucidated in the probability plot of Fig. 6. As shown, the lifetimes from the highest stresses exhibited a straight-line trend on the lognormal probability scale, while bimodal trends of the data tended to emerge at intermediate stress levels. As shown on an expanded scale in Fig. 7, the bimodal behavior was most evident for the fatigue datasets at $\sigma_{max}$ = 860 and 820 MPa. For each of these datasets, three regions of fatigue behavior are distinct (Type I, transition, and Type II), with the ratio of the data points in the Type I vs. Type II regions being stress–dependent. The transition points appear to represent the short-life region of the Type II behavior, indicating a substantial crack initiation lifetime. However, no standard probability density(s) adequately described the transition region, suggesting that the transition may represent a change in initiation mechanism. More work is required to clarify this speculation, however.

These separate regions of fatigue response were used as a basis for isolating the short- and long-life trends alone (eliminating the transition regions), as re-plotted in Fig. 8. As shown, when the Type I and Type II regions are plotted separately, the data appear nominally straight on the lognormal probability scale, indicating that each region is unimodal. Note that the data from the $\sigma_{max}$ = 860 and 820 MPa conditions are plotted twice, since both Type I and Type II regions were clearly present at these stress levels. In comparison with the full range of fatigue variability evident in the complete datasets of Fig. 6, Fig. 8 shows that the two regions of behavior tend to follow distinctly different trends, appearing to represent a life-limiting (Type I) behavior, plus a final period of fatigue exhaustion where all specimens eventually failed. Interestingly, in terms of the lognormal probability scale of the plot, there was limited variation of the slopes of the data at the individual stress levels in the two regions of behavior (life-limiting and fatigue–exhaustion), and the general slopes of the two regions were remarkably similar. Although all specimens failed (no run-out specimens), it appears that the longest-lived specimens may have been approaching a fatigue run-out of infinite lifetime.

Fig. 9 shows the data from the 820 MPa tests, and includes a lognormal probability regression line with 95% confidence intervals on the regression. Clearly, such a regression is inappropriate for bimodal data. However, materials and component designers rarely, if ever, have the luxury of having so many repeated tests at an individual fatigue condition. With fewer test results, the bimodal behavior would probably not be evident, and a regression

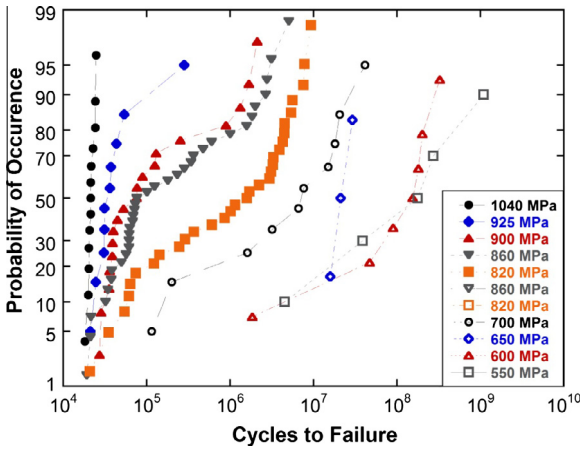


**Fig. 6.** Lognormal probability plot of fatigue lifetime data for individual stress levels shown in Fig. 5. From left to right: $\sigma_{max}$ = 1040, 925, 900, 860, 820, 700, 650, 600, and 550 MPa.

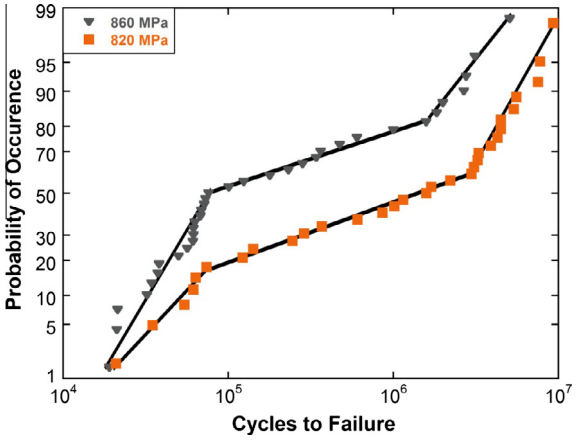


**Fig. 7.** Lognormal probability plot showing 820 MPa and 860 MPa data from Fig. 5, highlighting three regions of the bimodal trend (Type I, transition, Type II).

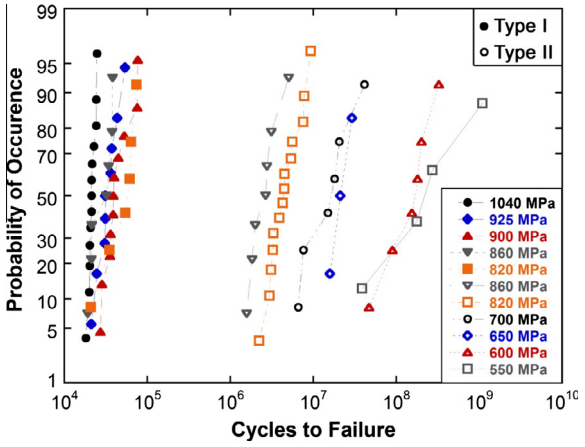


**Fig. 8.** Lognormal probability plot of Type I and Type II fatigue lifetime data alone for individual stress levels shown in Fig. 5. Note that 820 and 860 MPa data each appear twice, since these stress levels exhibited both Type I and Type II behavior. As shown in Fig. 6, data from 700 and 900 MPa tests also exhibited both types of behavior, but to a lesser extent than at 820 and 860 MPa.

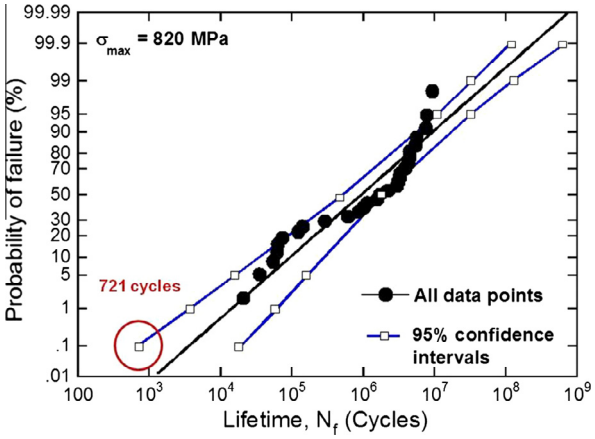


**Fig. 9.** Lognormal probability plot of lifetime data for tests with $\sigma_{max}$ = 820 MPa, showing a regression extrapolation to the B0.1 (1/1000) probability of failure, along with 95% confidence bands for the fit.

similar to the one shown would likely appear reasonable. In this case, one can see that extrapolation to the B0.1 probability of failure would give a lifetime of approximately 3500 cycles, while the corresponding lower bound of the 95% confidence interval was about 721 cycles. Alternatively, taking maximum benefit of the large number of data points at this condition allows one to focus on the single, short-life (Type I) distribution. Fig. 10 shows a probability plot of the 6 shortest-life data alone, and in this instance the estimated B0.1 life was greater than $10^4$ cycles, and the minimum 95% confidence estimate was approximately 5660 cycles, or about 8 times the corresponding value indicated by the unimodal analysis of the full data set. Thus, this example implies that existence of bimodal fatigue behavior may indicate that the material's inherent minimum lifetime is substantially greater than otherwise thought.

## 4. Analysis

### 4.1. Modeling bimodal fatigue

A key opportunity in the design of future materials is to understand, isolate, and model the sources of variability in fatigue damage and lifetime. As noted earlier, we previously established a general computational framework for physics-based understanding of fatigue variability [24,40]. In this approach, the lifetime distribution was modeled as a superposition of the probability densities of the crack-growth-dominated lifetime (Type I) and the crack-initiation-dominated, mean lifetime (Type II). The underlying initiation and cracking mechanisms for this material have been reported elsewhere, and a key factor in the fatigue variability of this material was microtexture [40–42,54–56]. The total lifetime density was represented by:

$$f_t(N) = p_l f_l(N) + p_m f_m(N) \tag{1}$$

where $f_t(N)$, $f_l(N)$, and $f_m(N)$ are probability densities representing the total lifetime, crack growth lifetime, and the mean, initiation-dominated lifetime, respectively. The factors, $p_l$ and $p_m$ are the probabilities of occurrence of the respective responses. Salient features of the model are (i) that the effect of any variable on lifetime distribution is separated into its influence on small-plus-large crack growth vs. the mean lifetime behaviors, and (ii) that the lifetime distribution is modeled as a superposition of these two responses. From a design life perspective (for example, a 1/1000, B0.1, lifetime), it can be shown that the prediction of life limit by the crack growth lifetime density, $f_l(N)$ (i.e., in the limit of $p_l = 1$) forms a lower bound of predictions by the bimodal model [35], as discussed below.

It is well known that the total fatigue life of a specimen is composed of the sum of the cycles from the successive stages of damage initiation and crack growth to failure, such that the total fatigue life ($N_T$) is given by:

$$N_T = N_i + N_{SC} + N_{LC} \tag{2}$$

where $N_i$, $N_{SC}$, and $N_{LC}$ are the cycles spent in crack initiation, small crack growth, and large-crack growth, respectively. It is also recognized that $N_i$ may be further subdivided into a crack-incubation plus a crack-nucleation phase in some instances, and that small cracks may be defined as being microstructurally, physically, mechanically, and/or chemically small [57–59]. For a given material and loading condition, the variability in total fatigue lifetime, $V_T$, is a sum of the variabilities of the individual stages of damage and cracking, and variability of the individual terms in Eq. (2) tends to reduce from left to right, such that $V(N_i) > V(N_{SC}) > V(N_{LC})$.

As noted earlier, for a typical 8000-cycle design life of turbine-engine rotor materials, the corresponding maximum stresses approach the material's yield stress. Under these circumstances, it appears that the number of cycles to crack initiation from a microstructural-scale feature approaches zero for the life-limiting fatigue. Assuming that $N_i \sim 0$, one can calculate the expected lifetime by integrating the equation:

$$N_T = 0 + \int_{a=a_i}^{a_{SC}} \frac{da}{f_{SC}(\Delta K)} + \int_{a_{SC}}^{a_f} \frac{da}{f_{LC}(\Delta K)} \tag{3}$$

where the two integrals represent the life spent in small-crack and large-crack growth, respectively, $a_i$ is the crack initiation depth from a microstructural or mechanical defect, $a_{SC}$ is the transition crack size between small- and large-crack growth, and $f_{SC}$ and $f_{LC}$ are the crack growth functions for the small- and large-crack size ranges, respectively. For the Monte Carlo model of the life-limiting fatigue process, the distribution of crack initiation sizes ($a_i$) was represented by the red curve of Fig. 11. For the data presented, $a_i$ was determined from a combination of surface measurements via standard acetate replica methods, combined with fractography of the crack initiating features, which were typically individual equiaxed primary α-phase particles ~4 um in diameter, such as the one shown in Fig. 4. Details on the initiation fractography are available in [39–41,52,55]. Analysis of the crack initiation sites revealed that the small cracks appeared to assume an approximately semicircular shape very quickly. As such, $a_i$ was defined as the

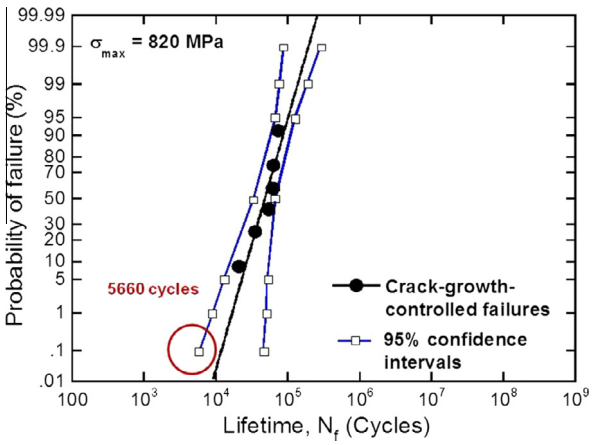


**Fig. 10.** Lognormal regression of the Type I, shortest-life, points alone, showing that the slope of the regression is much steeper and the B0.1 extrapolated life is much greater than shown from the full dataset in Fig. 8.

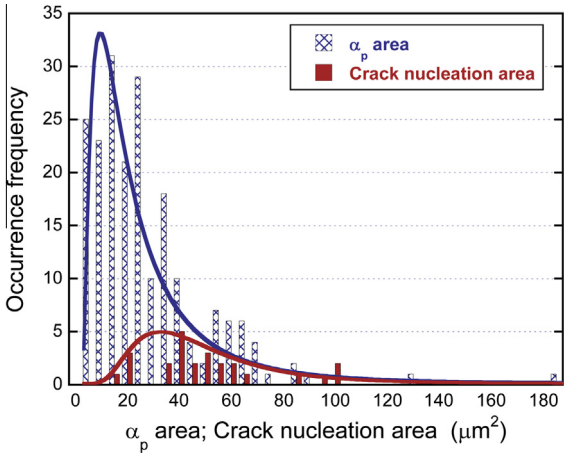


**Fig. 11.** Histograms of primary α particle sizes ($\alpha_p$) sizes (blue) as measured from metallurgical section and sizes of crack initiation regions (red) measured as projected normal to the fracture surface. (For interpretation of the references to colour in this figure legend, the reader is referred to the web version of this article.)

equivalent radius of the initiating feature, and the crack was assumed to be semicircular, since correlation with specific shapes of initiation particles was beyond the scope of the current project. General information on shape effects for small cracks in other materials is available in [60–64]. A statistical representation of the small-crack growth behavior shown in Fig. 12 ($R = 0.05$) was obtained using maximum likelihood methods to obtain a correlated Paris-law function to represent the variability in crack growth behavior, while the large-crack behavior was treated as deterministic (mean value). Since the small crack data were acquired at the same stress ratio as the smooth-bar fatigue specimens, no correction for $R$ was used. Moreover, since the small crack data exhibited no apparent threshold for crack growth ($\Delta K_{th}$), this value was assumed to be zero in the model calculations. For each stress level, at least 10,000 Monte Carlo simulations were used to calculate a distribution of expected minimum total lifetimes, assuming $N_i = 0$. The Monte Carlo simulation was implemented using Mathematica®, and the stress intensity factor calculation was based on the solution for a surface crack in a round bar given by Forman and Shivakumar [65]. The calculations assumed a single dominant crack, consistent with the experimental findings, and the failure criterion was based on the effective fracture toughness. Fig. 13 plots these predicted minimum lifetimes in comparison with the $\sigma_{max} = 820$ MPa life-limit data of Fig. 10. As shown, the probabilistic prediction agrees extremely well with the life-limit data, which tends to corroborate the assumption that $N_i$ was near zero for these tests.

Fig. 14 re-plots the $S$–$N$ data of Fig. 5, and shows a schematic of bimodal regressions of the fatigue behavior for each stress level. The three lines at the left of the plot represent Monte Carlo model predictions of the 0.1%, 10%, and 50% probabilities of failure, respectively, from left to right. As shown, all of the fatigue data are bounded approximately by the P(failure) = 10% line. In addition, the slopes of the Monte Carlo predictions vs. stress level agree well with the slope of the Type I fatigue lifetime line representing the behavior of the life-limiting populations alone, as defined by the linear behavior on a probability plot. Among the implications of the steeper slope for life-limiting fatigue is a reduced sensitivity to stress level, as compared to a traditional view of the mean $S$–$N$ fatigue behavior. Additional work is planned to explore, validate, and assess the generality of this apparent implication. This research includes work on micro-scale fatigue tests to help characterize modes of crystal plasticity leading to fatigue damage in the Ti-6246 material [66].

Also as shown in the figure, the proportions of data falling in the short- (Type I) vs. long-life (Type II) regions of $S$–$N$ behavior shift toward longer lifetimes as stress is reduced. Recalling Eq. (2), this is equivalent to reducing the probability ($p_I$) of a given fatigue data point being in the short life region. Based on a nonlinear bimodal regression of the fatigue data at each stress level, an estimate of the dependence of $p_I$ on stress level is plotted in Fig. 15. As shown, the maximum stress at which the short- and long-life behaviors become equally likely is approximately 820 MPa, which is about 79% of the yield strength for the Ti-6246 alloy tested.

Fig. 16a presents the results of 1000 Monte Carlo simulations of crack growth behavior at 820 MPa, and Fig. 16b shows an expanded region of the same plot. As shown, for the distribution of crack initiation depths (up to approximately 15 μm in this case), the minimum lifetime is more than 14,000 cycles, which is well in excess of the typical 8000 cycle (TAC) design lifetime. Recognizing that the estimate of $p_I$ at this stress level is 0.5, half of all specimens tested at this condition would be expected to lie within the short-life distribution. Since traditional low-cycle-fatigue safe-life design targets the 1/1000 statistical minimum for initiation of a 0.40 mm deep semicircular crack, this should correspond to the minimum values of the Monte Carlo predictions. As such, an alternative interpretation of the 1/1000, or −3 standard deviation, LCF safe-life criterion is that for these cases, in all likelihood, beginning at the size of a microstructural feature (~5–15 μm), a crack would have been growing for most of the safe-life period. There is a notable caveat in this regard, however, since the current results are for

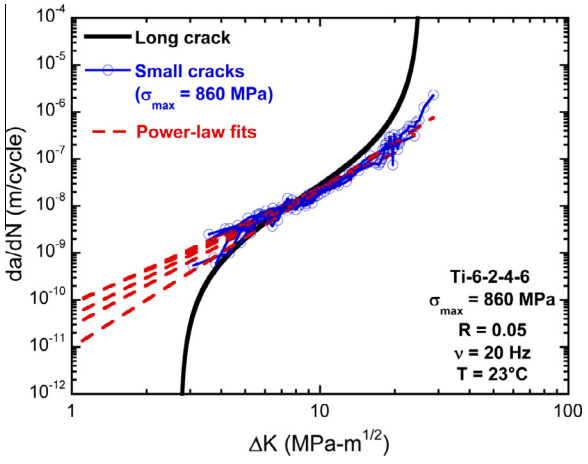


**Fig. 12.** Plot of d$a$/d$N$ vs. $\Delta K$ for several naturally initiated small surface cracks measured via acetate replication of the specimen surface, and regression trend from similar data on large cracks in conventional compact type C(T) specimens.

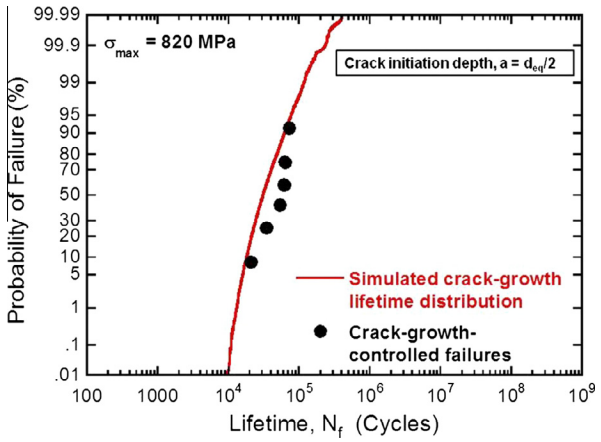


**Fig. 13.** Probability plot of Monte Carlo model simulation of Type I fatigue lifetimes based only on microstructure (Fig. 12) and small + large crack (Fig. 13) results plotted vs. the short life data from the $\sigma_{max} = 820$ MPa experiment (Fig. 9).

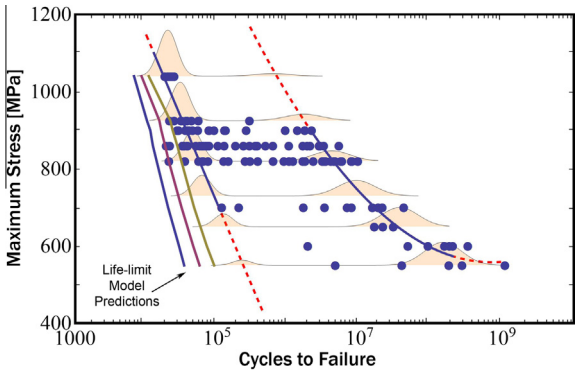


**Fig. 14.** $S$–$N$ plot showing (i) individual regression lines (blue and dashed) to Type I and Type II data, (ii) schematic bimodal probability distribution transitioning from Type I to Type II dominance with decreasing stress, and (iii) Monte Carlo predictions of 50%, 10%, and 0.1% probabilities of failure for the minimum lifetimes. (For interpretation of the references to colour in this figure legend, the reader is referred to the web version of this article.)

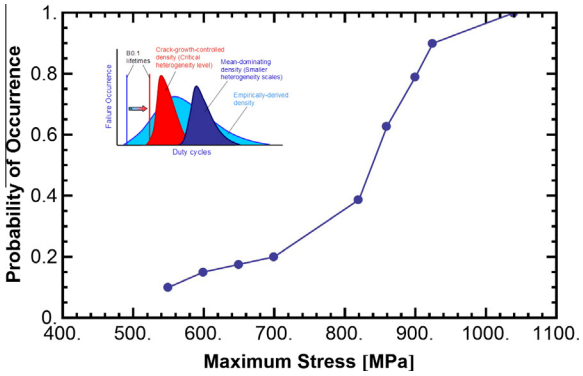


**Fig. 15.** Probability of occurrence of Type I (short-life) fatigue based on bimodal regression analysis of fatigue lifetime data from Fig 14.

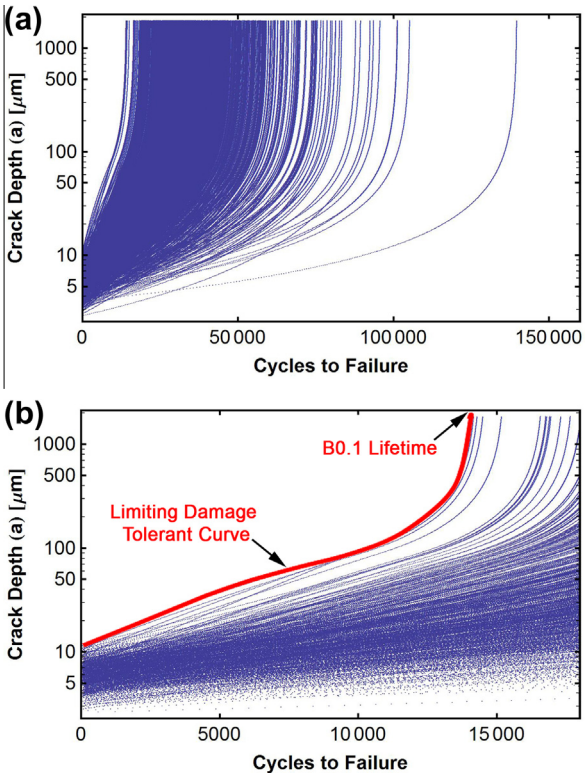


**Fig. 16.** (a) 1000 Monte Carlo model predictions of crack depth vs. life (a–N) for a maximum stress of 820 MPa, and (b) and the same predictions on an expanded scale that shows the area of primary interest for design and life management of rotor components designed to a total lifetime of 8000 cycles (TACs).

a stress-free surface condition, while actual components typically have highly compressive surface residual stresses from machining plus shot peening, as discussed below.

### 4.2. Effects of surface residual stresses produced by shot peening

Surface treatments such as shot peening are used widely to retard crack initiation and propagation in the surface region, and thereby increase the fatigue life. However, our findings from other research suggest that the effect of shot peening on the lifetime distribution should be represented in terms of its effect on the mean and the life-limiting behavior [42]. In work on the same Ti-6246 as reported in the current paper, shot-peening increased both the minimum and mean lifetimes by suppressing crack-initiation in the surface region and forcing crack-initiation to the subsurface in many samples [42]. Although failure by the subsurface mechanism improved the mean response, the life-limiting failures under shot-peening occurred by a different surface-crack-initiation mechanism in which cracking was found to originate as an interaction between shot-peening and the local microstructure, which created local regions of surface micro-cracking. These surface crack initiation sizes appeared to be significantly larger than the average primary α grain size (~4 μm) that controlled crack initiation in the residual stress free condition. The limiting lifetimes under shot peening were only about 1.7 times longer than those under the residual-stress free condition. In other words, a portion of the benefit from compressive surface residual stresses induced via shot peening was partially offset by the creation of surface cracks from shot peening damage. The primary benefit of the residual stress appeared to be due to the stresses acting perpendicular to the crack plane, which reduced the effective range of crack opening and stress intensity factor ($\Delta K_{eff}$).

### 4.3. Opportunities for improvement: sources of variability and uncertainty in material life limits

Given that life limits play such a crucial role in the design and management of turbine engine rotor materials, it appears that the results outlined in this paper represent a mere first step in the potential to reduce and model the variability in materials fatigue performance. By focusing on the mechanics and physics that control the short-life tail of a material's fatigue capability, it appears possible to characterize individual contributions to life limits with a high level of fidelity, potentially leading to increases in capabilities to control and fully utilize inherent materials properties. Two primary avenues for further development, maturation, and transition of the concepts of life-limiting fatigue are: (i) through the integrated design and certification of materials and structures for future systems and (ii) through improvements to methods of life-cycle management and prognosis.

As discussed above, beginning with the residual-stress-free case, one can start to isolate effects of microstructure on inherent fatigue variability. This special case presents the opportunity to identify life-limiting microstructural neighborhoods and effects of microstructural gradients on fatigue. As shown, the inherent life limits under low cycle fatigue appear to be governed by the growth of a dominant crack from an initial crack size given by the microstructural feature that controls crack formation. Thus, the approach of segmenting total lifetime into the components of initiation, small-, and large-crack growth offers a very systematic process for characterizing and modeling the many additional effects that are often difficult to quantify independently. Such models should provide new interpretations of fatigue behavior that have traditionally been based primarily on extrapolations from mean-fatigue properties. This could be significant in some instances, since minimum and mean fatigue responses differ based on microstructural and loading variables.

In light of the rapidly growing science and technology offered by Integrated Computational Materials Engineering, the modeling of life-limiting fatigue of materials presents many opportunities for the development, transition, and implementation of new understanding for both military and commercial applications, including:

- Quantitative 2- and 3-dimensional characterization and representation of life-limiting microstructural features vs. nominal and off-nominal microstructures, including characterization of microstructural hierarchies that control failure.
- Nondestructive characterization of materials deformation, damage states, microstructural features, and residual stresses.

- High resolution microscale testing of microstructural features, including digital image correlation for precision characterization of crystallographic mechanisms of deformation and damage.
- Crystal plasticity modeling of microstructural features, including life-limiting local neighborhoods and gradients.
- Analysis and modeling of effects of surface and bulk residual stresses.
- Effects of geometric stress concentrations, such as bolt holes and notches.
- 3-dimensional fracture mechanics of complex geometric features.
- Effects of complex mission loading and histories, including thermomechanical fatigue and dwell hold times.
- Advanced validation materials science, including selective analysis of the damage states of materials from retired components to provide model feedback and validation.
- Information integration and data mining.
- Methods for modeling uncertainty and confidence bounds in minimum fatigue life due to limited availability of data [67] and for statistical optimization of testing.
- Methods of material state awareness supporting condition based management + prognosis.
- Probabilistic modeling of multi-scale domains: microstructure, geometric feature, component, and system.
- Model-based probabilistic simulation and validation of materials and components designs.

## 5. Conclusions

This paper used electropolished specimens of the high-strength $\alpha + \beta$ titanium alloy Ti–6Al–2Sn–4Zr–6Mo to explore fundamental variabilities and uncertainties in microstructurally based fatigue life limits under stresses and lifetimes representative of engine rotor design (nominally 8000 major cycles, (TACs)). In this life range, it is well known that the total fatigue lifetime ($N_T$) may be partitioned as (Eq. (2)):

$$N_T = N_i + N_{SC} + N_{LC}$$

where $N_i$, $N_{SC}$, and $N_{LC}$ are, respectively, the numbers of cycles spent in crack initiation, small-crack growth, and large-crack growth to failure. In the test results presented here, $N_i$ was often the dominant term contributing to the mean fatigue lifetime, but the mean fatigue behavior sometimes also encompassed a shorter-life fatigue response wherein $N_i$ was small (approached zero). This minimum vs. mean bimodal fatigue behavior appeared to respond differently to stress level, which may be expected depending on the relative contribution of $N_i$ to the total fatigue lifetime. In related research, we have also observed that the trends in minimum vs. mean fatigue response may differ as a function of microstructural and usage variables.

For turbine-engine rotor materials, traditional design practice defines the safe-life fatigue limit as a statistical minimum life to form a small surface or corner crack. Alternatively, from a materials-microstructure perspective, one might define the minimum size of a small crack as the dimension of the microstructural features in which cracks initiate, which for the Ti-6246 alloy are primary alpha particles approximately 4 μm in diameter. Under the latter definition of cracking, our consistent results on repeated tests indicated that the minimum of $N_i$ approached 0 cycles, which meant that the minimum lifetime was spent almost completely in the growth of a crack that begins on the microstructural scale. Although the probability of occurrence of $N_i \to 0$ may be reduced by factors such as the imposition of surface residual stresses through shot peening, in the stress range of rotor design, it appears difficult to preclude the rare occurrence of secondary damage, which also leads to $N_i \to 0$.

Our research on Ti-6246 and other high performance materials suggests that the presumption of $N_i \to 0$ for rotor design stresses may be of general applicability. If this is correct, it may be attractive to reinterpret conventional approaches and strategies for life-cycle design and management of turbine-engine rotor materials and components.

## Acknowledgements

Financial support from the Air Force Office of Scientific Research (AFOSR) Structural Mechanics Program (Dr. David Stargel, Program Manager, Project # 11RX01COR) is gratefully acknowledged.

## References

[1] The_White_House. Advanced manufacturing partnership. <http://manufacturing.gov/amp/amp.html> [accessed: 13.06.12].
[2] US_Department_of_Defense. Engineered resilient systems: transforming engineering design to assure trustworthy and adaptive systems. <http://www.acq.osd.mil/chieftechnologist/areas/ers.html> [accessed: 06.12].
[3] The_White_House. Materials genome initiative: a renaissance of American manufacturing. <http://www.whitehouse.gov/blog/2011/06/24/materials-genome-initiative-renaissance-american-manufacturing> [accessed: 14.06.12].
[4] The_White_House. Big data research and development initiative. <http://www.whitehouse.gov/blog/2012/03/29/big-data-big-deal> [accessed: 14.06.12].
[5] Christodoulou L, Larsen JM. Using materials prognosis to maximize the utilization potential of complex mechanical systems. JOM 2004;56:15–9.
[6] Larsen JM, Christodoulou L. Integrating damage state awareness and mechanism-based prediction. JOM 2004;56:14.
[7] Larsen JM, Christodoulou L, Calcaterra JR, Dent ML, Derriso MM, Hardman WJ, Jones JW, Russ SM. In: Preface, materials damage prognosis – proceedings of a symposium of the materials science and technology 2004 conference; 2005.
[8] Larsen JM, Caton MJ, Jha SK, Rosenberger AH, John R, Buchanan DJ, Jira JR, Golden PJ. Understanding materials uncertainty for prognosis of advanced turbine engine materials. In: 51st AIAA/ASME/ASCE/AHS/ASC structures, structural dynamics and materials conference, Orlando, FL; 2010.
[9] US_Department_of_Defense, DoDI 4151.22. Condition based maintenance plus (CBM+) for materiel maintenance. <www.dtic.mil/whs/directives/corres/pdf/415122p.pdf>; 2007 [accessed: 08.01.12].
[10] Tuegel EJ, Ingraffea AR, Eason TG, Spottswood SM. Reengineering aircraft structural life prediction using a digital twin. Int J Aeros Eng 2011;2011.
[11] Proceedings of the 1st world congress on integrated computational materials engineering. ICME, in, Seven Springs, PA; 2011.
[12] National_Materials_Advisory_Board. Integrated computational materials engineering: a transformational discipline for improved competitiveness and national security, The National Academic Press; 2008.
[13] US_Air_Force. Technology horizons: a vision for air force science & technology during 2010–2030. <http://www.af.mil/information/technologyhorizons.asp> [accessed: 14.06.12].
[14] Southwest_Research_Institute. Design assessment of reliability with INspection (DARWIN). <http://www.darwin.swri.org/> [accessed: 06.12].
[15] Reinman G, Ayer T, Davan T, Devore M, Finley S, Glanovsky J, et al. Design for variation. Qual Eng 2012;24:317–45.
[16] Kacprzynski G, Sarlashkar A, Roemer M, Hess A, Hardman B. Predicting remaining life by fusing the physics of failure modeling with diagnostics. JOM J Minerals, Metals Mater Soc 2004;56:29–35.
[17] The_National_Academies. Examination of the US Air Force's aircraft sustainment needs in the future and its strategy to meet those needs, natl academy pr. <http://www.nap.edu/catalog.php?record_id=13177, 2011> [accessed: 08.01.13].
[18] US_Department_of_Defense. Propulsion system integrity program (PSIP). www.everyspec.com [accessed: 14.06.12].
[19] US_Air_Force. MIL-HDBK-1783B (W/CHANGE 2), DEPARTMENT OF DEFENSE HANDBOOK: ENGINE STRUCTURAL INTEGRITY PROGRAM (ENSIP). <http://www.everyspec.com/MIL-HDBK/MIL-HDBK-1500-1799/MIL-HDBK-1783B_CHG-2_26101/>; 2004.
[20] Federal_Aviation_Administration. AC 33.14-1 – damage tolerance for high energy turbine engine rotors. <http://www.faa.gov/regulations_policies/advisory_circulars/index.cfm/go/document.information/documentID/22920> [accessed: 14.06.12].
[21] Cashman GT. A mathematical model for competing failure modes in strain cycle fatigue. J Eng Mater Technol, Trans ASME 2007;129:293–303.
[22] Cashman GT. A statistical methodolgy for the preparation of a competing modes fatigue design curve. J Eng Mater Technol, Trans ASME 2007;129:159–68.
[23] Jha SK, Caton MJ, Rosenberger AH, Li K, Porter WJ. Superimposing mechanisms and their effect on the variability in fatigue lives of a nickel-based superalloy.

In: Larsen JM, Christodoulou L, Calcaterra JR, Dent ML, Derriso MM, Hardman WJ, Wayne Jones J, Russ SM editors. Materials damage prognosis – a symposium of the materials science and technology 2004 conference, New Orleans, LA; 2005. p. 343–50.
[24] Jha SK, Caton MJ, Larsen JM. Mean vs. life-limiting fatigue behavior of a nickel-based superalloy. In: 11th International symposium on superalloys, superalloys 2008, Champion, PA; 2008. p. 565–72.
[25] Porter II WJ, Li K, Caton MJ, Jha S, Bartha BB, Larsen JM. Microstructural conditions contributing to fatigue variability in P/M nickel-base superalloys. In: 11th International symposium on superalloys, superalloys 2008, Champion, PA; 2008. p. 541–8.
[26] Caton MJ, Jha SK. Small fatigue crack growth and failure mode transitions in a Ni-base superalloy at elevated temperature. Int J Fatigue 2010;32:1461–72.
[27] Przybyla CP, McDowell DL. Simulation-based extreme value marked correlations in fatigue of advanced engineering alloys. In: 10th International fatigue congress, FATIGUE 2010, Prague; 2010. p. 1045–56.
[28] Przybyla C, Prasannavenkatesan R, Salajegheh N, McDowell DL. Microstructure-sensitive modeling of high cycle fatigue. Int J Fatigue 2010;32:512–25.
[29] Przybyla CP, McDowell DL. Microstructure-sensitive extreme value probabilities for high cycle fatigue of Ni-base superalloy IN100. Int J Plast 2010;26:372–94.
[30] Brogdon ML, Rosenberger AH. Evaluation of the influence of grain structure on the fatigue variability of waspaloy. In: 11th International symposium on superalloys, superalloys 2008, Champion, PA; 2008. p. 583–8.
[31] Morrissey RJ, John R, Porter II JW. Fatigue variability of a single crystal superalloy at elevated temperature. Int J Fatigue 2009;31:1758–63.
[32] Jha SK, Chandran KSR. An unusual fatigue phenomenon: duality of the *S–N* fatigue curve in the β-titanium alloy Ti–10V–2Fe–3Al. Scripta Mater 2003;48:1207–12.
[33] Ravi Chandran KS, Jha SK. Duality of the *S–N* fatigue curve caused by competing failure modes in a titanium alloy and the role of poisson defect statistics. Acta Mater 2005;53:1867–81.
[34] Ravi Chandran KS. Duality of fatigue failures of materials caused by poisson defect statistics of competing failure modes. Nat Mater 2005;4:303–8.
[35] Jha SK, Larsen JM, Rosenberger AH, Hartman GA. Dual fatigue failure modes in Ti–6Al–2Sn–4Zr–6Mo and consequences on probabilistic life prediction. Scripta Mater 2003;48:1637–42.
[36] Jha SK, Larsen JM, Rosenberger AH, Hartman GA. Mechanism-based variability in fatigue life of Ti–6Al–2Sn–4Zr–6Mo. ASTM Special Tech Publication 2004;1450:116–27.
[37] Szczepanski CJ, Shyam A, Jha SK, Torbet CJ, Johnson SJ. Characterization of the role of microstructure on the fatigue life of Ti–6Al–2Sn–4Zr–6Mo using ultrasonic fatigue. In: Larsen JM, Christodoulou L, Calcaterra JR, Dent ML, Derriso MM, Hardman WJ, Wayne Jones J, Russ SM, editors. Materials damage prognosis – a symposium of the materials science and technology 2004 conference, New Orleans, LA; 2005. p. 315–20.
[38] Annis CG, Larsen JM, Rosenberger AH, Jha SK, Annis DH. RFTh, a random fatigue threshold probability density for Ti6246. In: Larsen JM, Christodoulou L, Calcaterra JR, Dent ML, Derriso MM, Hardman WJ, Wayne Jones J, Russ SM, editors. Materials damage prognosis – a symposium of the materials science and technology 2004 conference, New Orleans, LA; 2005. p. 151–6.
[39] Jha SK, Larsen JM. Random heterogeneity scales and probabilistic descrdption of the long-lifetime regime of fatigue. In: 4th International conference on very high cycle fatigue, VHCF-4, Ann Arbor, MI; 2007. p. 385–96.
[40] Jha SK, Caton MJ, Larsen JM. A new paradigm of fatigue variability behavior and implications for life prediction. Mater Sci Eng A 2007;468–470:23–32.
[41] Szczepanski CJ, Jha SK, Larsen JM, Jones JW. Microstructural influences on very-high-cycle fatigue-crack initiation in Ti-6246. Metal Mater Trans A: Phys Metall Mater Sci 2008;39:2841–51.
[42] Jha SK, John R, Larsen JM. Nominal vs local shot-peening effects on fatigue lifetime in Ti–6Al–2Sn–4Zr–6Mo at elevated temperature. Metall Mater Trans A: Phys Metall Mater Sci 2009;40:2675–84.
[43] Golden PJ, Millwater HR, Yang X. Probabilistic fretting fatigue life prediction of Ti–6Al–4V. Int J Fatigue 2010;32:1937–47.
[44] Ravi Chandran KS, Chang P, Cashman GT. Competing failure modes and complex *S–N* curves in fatigue of structural materials. Int J Fatigue 2010;32:482–91.
[45] McDowell DL, Dunne FPE. Microstructure-sensitive computational modeling of fatigue crack formation. Int J Fatigue 2010;32:1521–42.
[46] Jha SK, Szczepanski CJ, Golden PJ, Porter WJ, John R. Characterization of fatigue crack-initiation facets in relation to lifetime variability in Ti–6Al–4V. Int J Fatigue 2012;42:248–57.
[47] Caton MJ, John R, Porter WJ, Burba ME. Stress ratio effects on small fatigue crack growth in Ti–6Al–4V. Int J Fatigue 2012;38:36–45.
[48] Jha SK, Larsen JM, Rosenberger AH. The role of competing mechanisms in the fatigue-life variability of a titanium and gamma-TiAl alloy. JOM 2005;57:50–4.
[49] Jha SK, Larsen JM, Rosenberger AH. The role of competing mechanisms in the fatigue life variability of a nearly fully-lamellar γ-TiAl based alloy. Acta Mater 2005;53:1293–304.
[50] Buchanan DJ, Larsen JM, Rosenberger AH, Jha SK, Hutson AL, Blosser PE, et al. Reducing uncertainty for fatigue life limits at notches in two structural alloys. In: TMS 2012 annual meeting & exhibition, presentation: TMS 2012 annual meeting & exhibition, Orlando, FL; 2012.
[51] Frost N, Marsh K, Pook L. Metal fatigue. Clarendon, Oxford; 1974. p. 417–21.
[52] Jha SK, Larsen JM, Rosenberger AH. Towards a physics-based description of fatigue variability behavior in probabilistic life-prediction. Eng Fract Mech 2009;76:681–94.
[53] Rosenberger AH, Buchanan DJ, Ward DA, Jha SK. The variability of fatigue in notched bars of IN100. In: Superalloys 2012, TMS, Seven Springs, PA; 2012. p. 143–148.
[54] Szczepanski CJ, Jha SK, Larsen JM, Jones JW. The role of microstructure on the fatigue lifetime variability in an α + β titanium alloy, Ti–6Al–2Sn–4Zr–6Mo. In: 4th International conference on very high cycle fatigue, VHCF-4, Ann Arbor, MI; 2007. p. 37–44.
[55] Szczepanski CJ, Jha SK, Larsen JM, Jones JW. The role of local microstructure on small fatigue crack propagation in an $\alpha + \beta$ titanium alloy, Ti–6Al–2Sn–4Zr–6Mo. Metall Mater Trans A: Phys Metall Mater Sci 2012:4097–112.
[56] Jha SK, John R, Larsen JM. Incorporating small fatigue crack growth in probabilistic life prediction: effect of stress ratio in Ti–6Al–2Sn–4Zr–6Mo. Int J Fatigue; in press, http://dx.doi.org/10.1016/j.ijfatigue.2013.01.008.
[57] Ritchie R, Lankford J. Small fatigue cracks: a statement of the problem and potential solutions. Mater Sci Eng 1986;84:11–6.
[58] Suresh S, Ritchie R. Propagation of short fatigue cracks. Int Mater Rev 1984;29:445–75.
[59] Ritchie R. Mechanisms of fatigue crack propagation in metals, ceramics and composites: role of crack tip shielding. Mater Sci Eng: A 1988;103:15–28.
[60] Ravichandran KS, Larsen JM. Microstructure and crack-shape effects on the growth behavior of small fatigue cracks in Ti24Al11Nb. Mater Sci Eng A 1992;153:499–507.
[61] Burns JT, Larsen JM, Gangloff RP. Driving forces for localized corrosion-to-fatigue crack transition in Al–Zn–Mg–Cu. Fatigue Fract Eng Mater Struct 2011;34:745–73.
[62] Burns JT, Larsen JM, Gangloff RP. Effect of initiation feature on microstructure-scale fatigue crack propagation in Al–Zn–Mg–Cu. Int J Fatigue 2012;42:104–21.
[63] Ravichandran K. Effects of crack aspect ratio on the behavior of small surface cracks in fatigue: Part I. Simul, Metall Mater Trans A 1997;28:149–56.
[64] Ravichandran KS, Larsen JM. Effects of crack aspect ratio on the behavior of small surface cracks in fatigue: Part II. Experiments on a titanium (Ti–8Al) alloy. Metall Mater Trans A: Phys Metall Mater Sci 1997;28:157–69.
[65] Forman RG, Shivakumar V. Growth behavior of surface cracks in the circumferential plane of solid and hollow cylinders. In: Fracture mechanics: seventeenth volume: seventeenth national symposium on fracture mechanics on fracture mechanics sponsored astm committee e-24 on fracture testing, Albany, New York, 7–9 August 1984, Astm Intl; 1986. p. 59.
[66] Szczepanski CJ, Jha SK, Shade PA, Wheeler R, Larsen JM. Demonstration of an in situ microscale fatigue testing technique on a titanium alloy. Int J Fatigue; in press, http://dx.doi.org/10.1016/j.ijfatigue.2012.08.008.
[67] Golden PJ, Larsen JM, John R, Jha SK. Confidence bound estimation for mechanism-based small crack growth probabilistic design life predictions. In: ASME turbo expo 2013, power for land, sea, and air, San Antonio, TX; 2013.